

# Potential Flow Analysis of Multielement Airfoils Using Conformal Mapping

N. D. Halsey\*

*Douglas Aircraft Company, Long Beach, Calif.*

Conformal mapping techniques are applied to the problem of calculating the two-dimensional potential flow about multielement airfoils. Airfoil geometry is completely arbitrary and, unlike other mapping methods, any number of airfoil elements can be considered. The multiple airfoil elements are transformed to the same number of circles by successive applications of a method for mapping a single body to a unit circle. The flow about the multiple circles is analyzed using multiply-reflected doublets and vortices. All iterative procedures converge rapidly, giving accurate results with considerably better computational efficiency than existing distributed-singularity panel methods.

## Introduction

FOR many years, conformal mapping techniques have been used for two-dimensional potential flow calculations. They are used most commonly to generate special exact solutions for evaluating the accuracy of more general numerical techniques, such as the distributed-singularity methods. Examples of such applications include Joukowski airfoils, Karman-Trefftz airfoils, and other classical single-element airfoils and, more recently, some two-element airfoils generated by Williams<sup>1</sup> and James.<sup>2</sup> Conformal mapping techniques are also used, but less frequently, for design problems requiring the analysis of the flow about airfoils of more general shape. The methods developed by Theodorsen<sup>3</sup> and James<sup>4</sup> can analyze flows about single-element airfoils of nearly arbitrary shape. The methods developed by Garrick<sup>5</sup> and Ives<sup>6</sup> can analyze flows about two-element airfoils of nearly arbitrary shape. Although these more general conformal mapping methods can no longer be regarded as exact, since they use truncated infinite series and make other numerical approximations, they are nevertheless highly accurate. They also have a high degree of computational efficiency. The more modern methods,<sup>4,6</sup> which make use of the Fast Fourier Transform,<sup>7</sup> appear to be significantly more efficient than the distributed-singularity methods, which must form, store, and solve very large matrices of linear algebraic equations. In the past, however, there have been no conformal mapping techniques capable of analyzing flows about general multielement airfoils having more than two elements. In the author's opinion, this limitation has been largely responsible for the widespread preference for distributed-singularity methods over conformal mapping methods for two-dimensional potential flow analysis.

This paper describes a new potential flow method based on conformal mapping and using Fast Fourier Transforms. Unlike previous mapping methods, completely arbitrary multielement airfoils (with any number of elements) can be

analyzed. In this method, the multiple airfoil components are transformed to the same number of disjoint circles. The flow solution is calculated in the multiple-circle plane and then transformed back to the original (physical) plane. Preliminary results obtained to date indicate that the accuracy is very good and that the computational expense can be perhaps an order of magnitude less than that of existing distributed-singularity methods. The following sections describe the general theory and some of the details of the numerical calculations and present results for cases having up to four elements. More detailed information on most parts of the method can be found in Ref. 8.

## Formulation of the Problem and Its Solution Using Conformal Mapping

The general problem of calculating the inviscid, incompressible, two-dimensional flow about multielement airfoils requires the solution of Laplace's equation ( $\nabla^2 \phi = 0$ ) for the velocity potential  $\phi$ , with boundary conditions of zero normal velocity component on all solid surfaces ( $V_n = 0$ ), and zero velocity perturbation at large distances from the airfoil elements ( $V_\infty = \text{const}$ ). Auxiliary conditions (Kutta conditions) are also imposed to fix the value of the circulation about each airfoil element, usually by requiring the trailing-edge velocity to be the same whether approached from the upper or lower surfaces.

Now suppose the problem, as just posed, is transformed by applying any number of conformal mappings. Denote the complex coordinates in the original (untransformed) plane by  $z$  and in the final (transformed) plane by  $\zeta$ . The mapping function between the two planes [ $z(\zeta)$ ] is an analytic function of  $\zeta$ . The mapping derivative ( $dz/d\zeta$ ) of the overall transformation consists of the product of the mapping derivatives for each mapping performed. It is shown in numerous texts that the gradient and Laplacian of a scalar field transform as:

$$\nabla \phi(z) = \frac{\nabla \phi(\zeta) dz/d\zeta}{|dz/d\zeta|^2} \quad (1)$$

$$\nabla^2 \phi(z) = \frac{\nabla^2 \phi(\zeta)}{|dz/d\zeta|^2} \quad (2)$$

As a consequence of Eq. (1), normal and tangential velocity components transform as

$$v_n(z) = \frac{v_n(\zeta)}{|dz/d\zeta|} \quad (3)$$

Presented as Paper 79-0271 at the AIAA 17th Aerospace Sciences Meeting, New Orleans, La., Jan. 15-17, 1979; submitted Jan. 29, 1979; revision received June 26, 1979. Copyright © American Institute of Aeronautics and Astronautics, Inc., 1979. All rights reserved. Reprints of this article may be ordered from AIAA Special Publications, 1290 Avenue of the Americas, New York, N.Y. 10019. Order by Article No. at top of page. Member price \$2.00 each, nonmember, \$3.00 each. Remittance must accompany order.

Index categories: Aerodynamics; Computational Methods; Subsonic Flow.

\*Senior Engineer/Scientist, Aerodynamics Research. Member AIAA.

$$v_t(z) = \frac{v_t(\xi)}{|dz/d\xi|} \quad (4)$$

Circulation is unaffected by a conformal transformation.

The transformed flow problem is thus very similar to the original flow problem. The general field equation and normal-velocity boundary condition are unchanged. The condition requiring zero-flow perturbation at large distances from the airfoil is unchanged if the transformation satisfies the condition

$$\lim_{|z| \rightarrow \infty} \left( \frac{dz}{d\xi} \right) = 1 \quad (5)$$

The Kutta conditions are also unchanged if the mapping derivative of the transformation is continuous across the trailing edge of each element. If the transformed shapes have no trailing-edge corners, then the Kutta conditions can be satisfied by specifying zero tangential velocity component at the trailing edges of the transformed airfoil elements.

A practical solution thus involves two nearly independent parts—the determination of the mapping function and mapping derivative of the transformation and the solution of the flow problem in the transformed plane. The general character of the transformed plane is chosen in such a way that the flow solution is easier (the boundary conditions are more easily applied) in the transformed plane than the untransformed plane. Velocity components in the physical plane are then found using Eqs. (1) and (4).

### Conformal Mapping of Multielement Airfoils

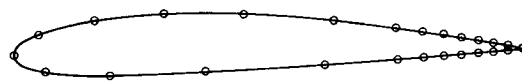
#### General Approach

One major difficulty in developing a conformal mapping method for general multielement airfoils is the choice of a suitable mapped domain. In the case of single-element airfoils, Riemann's mapping theorem insures that any body can be mapped to a unit circle. Thus, choice of the mapped domain is trivial. For two-element airfoils, a similar result insures that the region outside the two elements can be mapped to the annular region between two concentric circles. There is only one unknown parameter—the ratio of the radii of the circles—characterizing the mapped domain. According to Nehari,<sup>9</sup> however, there are  $3NB - 6$  parameters ( $NB$  is the number of airfoil elements) required to characterize the mapped domain, whatever its general form may be, of multielement airfoils having more than two elements. The determination of the geometry in the transformed plane and the mapping function between the physical and transformed planes is, accordingly, much more difficult.

However, two observations of elementary single-body mappings can be made which, at the same time, suggest a natural form for the mapped domain to take and a simple procedure for actually carrying out the mapping. The first observation concerns Joukowski and Karman-Trefftz mappings. It is well known that application of either of these transformations to a circle can result in a shape closely resembling a realistic airfoil. It is also true that application of the inverse of either of these mappings to a real airfoil can remove the trailing-edge corner and result in a shape closely resembling a circle. This is illustrated in Fig. 1, which shows an NACA 2412 airfoil and the quasicircular shape which results from applying the inverse Karman-Trefftz mapping. The second observation is that, for transformations satisfying Eq. (5), the distortions of the domain are strongly localized near the single body. This is illustrated in Fig. 2, which shows the distortion of a number of concentric circles resulting from the mapping of one of them to a flat plate.

From these two observations, the basis of a practical multielement mapping procedure emerges. First, use the inverse Karman-Trefftz mapping to remove the trailing-edge corner (or any other corner) from one of the airfoil elements.

PHYSICAL GEOMETRY



MAPPED GEOMETRY

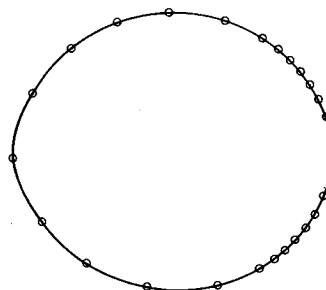
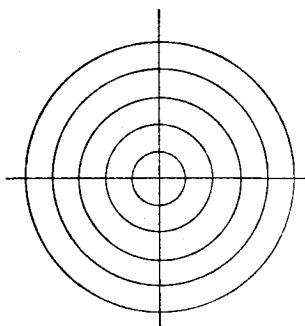


Fig. 1 Effect of the corner-removing mapping on the shape of a single-element airfoil (NACA 2412).

CONCENTRIC CIRCLES



MAPPED IMAGES OF THE CONCENTRIC CIRCLES

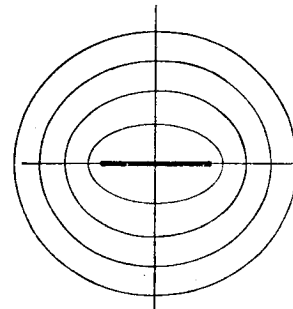


Fig. 2 Locality of the distortion caused by a conformal mapping—mapping the smallest of several concentric circles onto a flat plate.

This makes that element quasicircular and distorts the other elements to various degrees depending on their proximity to the first element. Then repeat the corner-removing process for each element having a corner. At this point, all elements are quasicircular, or at least more nearly circular than before the corner-removing mappings. The next step is to map one of the elements to a unit circle and calculate the distortion that this causes to the shapes of the other elements. Then repeat the single-element mapping process until it has been applied once to each element. At this point, the last element is a unit circle and the other elements (having once been circles) are much more nearly circular than immediately after the corner-removing process. The single-element mappings are again applied successively to each element, as many times as necessary, until all elements are sufficiently close to circular in shape. The area outside the multiple elements in the physical plane is thus transformed to the area outside the same number of disjoint circles. The transformation is done without the previous knowledge of any of the  $3NB - 6$  parameters characterizing the mapped domain and with no mathematics more complicated than that required for single-element mappings.

#### Numerical Considerations Affecting the General Approach

The general approach can be summarized as a succession of inverse Karman-Trefftz mappings to remove all corners, followed by a succession of single-body mappings, each of which maps a smooth body with no corners onto a unit circle.

The single-body mapping method used in this particular application is derived from the method developed by James,<sup>4</sup> which is quite capable of removing a corner from a body and transforming it to a circle all in one step. This capability was not used for reasons explained in the next paragraph.

In order to calculate the mapping derivative of the overall transformation, the mapping derivatives of the individual mappings must be multiplied together. In any approach, some numerical interpolation is required in order to make the results of consecutive mappings refer to the same points. In this approach, all interpolations give results at points corresponding to the original defining points. Figure 3 shows the variation of the modulus of the mapping derivative around the perimeter of an airfoil when it is mapped to a circle and when it simply has a corner-removing mapping applied to it. Almost all the character to the curve for the overall mapping derivative is provided by the corner-removing mapping alone. The present approach avoids interpolating the more rapidly varying results of the corner-removing mappings, thereby minimizing the magnitude of any numerical errors introduced by the interpolations.

Each single-body mapping used in this procedure requires as given information the variation of surface angle with arc length around the perimeter of the body being mapped. These quantities obviously can be determined by fitting curves through the points defining the bodies. In this application, however, such numerical curve fits are used only to process the geometry in the initial (physical) plane. Thereafter, the mapping parameters of each mapping (including the corner-removing mappings) are used to update analytically the required geometric data. Because of this and the separation of the corner-remover and circle mappings described in the previous paragraph, the number of significant terms in the infinite series for the mapping function of each individual single-body mapping can be much smaller than would otherwise be required. As a result, this approach is numerically very accurate and computationally very efficient.

#### Corner-Removing Mapping Procedure

The Karman-Trefftz transformation

$$\left( \frac{z - z_0}{z - z_1} \right) = \left( \frac{\xi - \beta z_0}{\xi - \beta z_1} \right)^{1/\beta} \quad (6)$$

can be used to transform a body with a corner in the  $z$  plane to a body without a corner in the  $\xi$  plane. In Eq. (6),  $z_0$  is the location of the corner in the  $z$  plane,  $z_1$  is the location of a singular point within the body, and  $\beta$  represents the parameter  $[1/(2 - \tau/\pi)]$ , where  $\tau$  is the included angle of the corner. The transformation is nonunique, since the internal singular point can be located arbitrarily. In the present application, this point is located halfway between the point of maximum curvature at the leading edge and its center of curvature. Other locations could be used, but usually would result in more severe bumps or depressions in the transformed body. If the body has a sharp leading edge with the same included angle as the trailing edge, both corners can be removed simultaneously by placing  $z_1$  at the location of the new corner. Thus, zero-thickness airfoils may be analyzed as easily as thick airfoils. Equation (6) can be rearranged and differentiated to give simple expressions for  $\xi$  and  $dz/d\xi$  in terms of known quantities. In a coordinate system which has been translated to make  $z_0 = 0$ ,

$$\xi = \beta z_1 \left[ 1 - \left( \frac{z - z_1}{z} \right)^\beta \right]^{-1} \quad (7)$$

$$\frac{dz}{d\xi} = \frac{z^2}{\xi^2} \left( \frac{z - z_1}{z} \right)^{1-\beta} \quad (8)$$

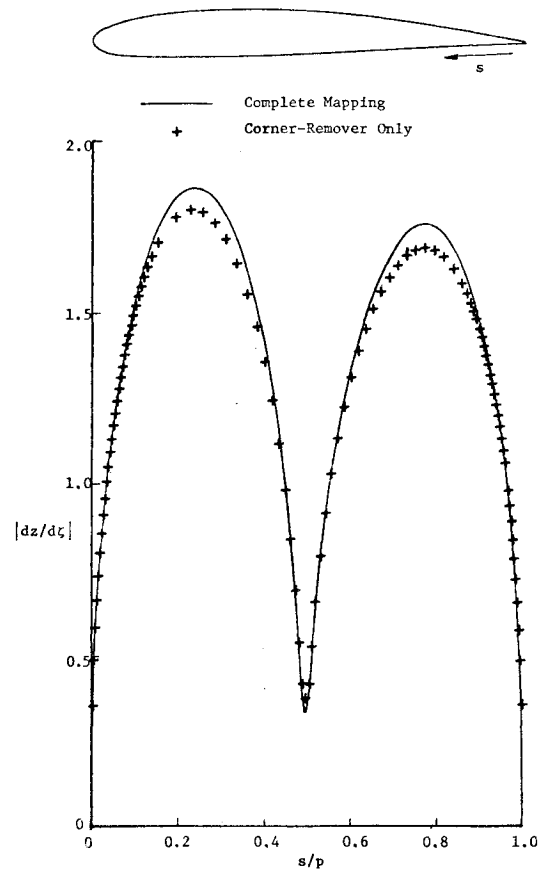


Fig. 3 Mapping derivative on a single-element airfoil (NACA 2412).

In order to keep track of the proper quadrants for the arguments of the fractional powers of  $z$  and  $(z - z_1)$ , a tracking procedure which insures that the arguments of these quantities vary continuously from point to point and body to body is employed.

Ives<sup>6</sup> has developed an alternative method which allows any number of airfoils to be transformed to the same number of bodies without corners simultaneously (rather than successively). This requires an iterative solution procedure which becomes more difficult as the number of bodies increases. Presently, it is not clear whether or not Ives' method is more efficient than the present one.

#### Single-Element Mapping Procedure

The single-element mapping method used in the present application of the general multielement mapping approach is based on the method developed by James.<sup>4</sup> This method makes full use of the power of Fast Fourier Transform techniques and has proven to be very fast and accurate.<sup>10</sup> Of the alternate methods that could have been used, Sells' method<sup>11</sup> is much less efficient, since it does not use Fast Fourier Transforms, and Theodorsen's method<sup>3</sup> is perhaps less general, since it is known to fail for bodies that are not sufficiently close to circular. The description given below assumes that the body to be mapped can be represented by a continuous closed curve with no corners, although these restrictions are not inherent in James' basic approach.

In this method, the region outside a smooth closed curve in one plane  $z$  is transformed conformally to the region outside a unit circle in another plane  $\xi$ . The trailing-edge point of the body in the  $z$  plane is assumed to transform to the point  $\xi = 1$ . Distant portions of the  $z$  and  $\xi$  planes are assumed to be identical in both scale and angular orientation. Since the mapping derivative of a conformal transformation is an analytic function, it can be expanded in an infinite series

having the form

$$\frac{dz}{d\zeta} = a_0 + \frac{a_1}{\zeta} + \frac{a_2}{\zeta^2} + \dots \quad (9)$$

where  $a_0, a_1, a_2, \dots$  are complex coefficients. The correspondence between distant portions of the  $z$  and  $\zeta$  planes fixes the value of  $a_0$  ( $a_0 = 1.0$ ). Body closure constraints fix the value of  $a_1$  ( $a_1 = 0.0$ ).

In order to facilitate the derivation of computationally useful relationships, another series (for the natural logarithm of the mapping derivative) is introduced

$$\ln \frac{dz}{d\zeta} = b_0 + \frac{b_1}{\zeta} + \frac{b_2}{\zeta^2} + \dots \quad (10)$$

The coefficients of this series are related to the coefficients of the series in Eq. (9) by a simple recursion formula given in Ref. 8 and elsewhere. In particular, however, the restrictions on  $a_0$  and  $a_1$  constrain the first two coefficients to be  $b_0 = b_1 = 0.0$ .

On the surface of a unit circle in a system having an angular coordinate  $\omega$  measured clockwise from the positive  $x$  axis, the coordinates are given by  $\zeta = e^{-i\omega}$ . Substituting this result in Eq. (10) gives

$$\ln \frac{dz}{d\zeta} = b_0 + b_1 e^{i\omega} + b_2 e^{i2\omega} + \dots \quad (11)$$

In order to apply Fast Fourier Transforms, this series must be truncated. In the present method, only base 2 transforms are used, since these are the simplest and most efficient. This restricts the number of possible terms in the series to numbers such as 17, 33, 65, 129, etc., and the number of discrete points on the unit circle to numbers such as 33, 65, 129, 257, etc.

The use of Eq. (11) and elementary relationships allows the derivation of the following equations:

$$\ln \left| \frac{dz}{d\zeta} \right| = R\{b_0 + b_1 e^{i\omega} + b_2 e^{i2\omega} + \dots\} \quad (12)$$

$$\arg \frac{dz}{d\zeta} = \theta + \omega - \frac{3\pi}{2} = I\{b_0 + b_1 e^{i\omega} + b_2 e^{i2\omega} + \dots\} \quad (13)$$

where  $\theta$  denotes surface angle in the  $z$  plane, and  $R$  and  $I$  denote real and imaginary parts, respectively, of a complex number. These relationships allow the following iteration procedure to be used to calculate the coefficients of the series in Eq. (11):

1) Estimate the values of  $\ln |dz/d\zeta|$  at equally spaced points on the unit circle and integrate them numerically with respect to  $\omega$  to find estimates of the arc lengths at body points corresponding to equally-spaced points on the circle.

2) Interpolate the geometric data of the body to determine the surface angles at these points. Then use Eq. (13) to find estimates of the values of  $\arg(dz/d\zeta)$  at the points on the circle.

3) Apply two successive Fast Fourier Transform calculations—the first of which uses the estimates of  $\arg(dz/d\zeta)$  to find estimates of the values of the coefficients in Eq. (11), and the second of which uses these coefficients (modified by the constraints  $b_0 = b_1 = 0$ ) to provide updated estimates of the values of  $\ln |dz/d\zeta|$ .

4) Repeat steps 1-3 until convergence is obtained. (This typically requires 10-20 iterations.)

Given the coefficients of the series in Eq. (11), the coefficients in Eq. (9) are found easily and integrated to obtain another series for the mapping function itself.

$$z(\zeta) = \zeta + c_0 + \frac{c_1}{\zeta} + \frac{c_2}{\zeta^2} + \dots \quad (14)$$

The series can be evaluated using Fast Fourier Transforms to give the coordinates in the  $z$  plane corresponding to equally spaced points in the  $\zeta$  plane. Alternatively, the surface arc lengths of these points can be calculated by the numerical evaluation of the integral  $\oint |dz/d\zeta| d\omega$ . These arc lengths can be used to interpolate for the coordinates in the  $z$  plane corresponding to the equally spaced points in the  $\zeta$  plane or to interpolate for the coordinates in the  $\zeta$  plane corresponding to the defining points in the  $z$  plane.

It is possible to transform a body to a unit circle without affecting the scale of distant portions of the field only if the body is of a particular size. Since the only geometric parameters required in this mapping method are the surface angles and normalized arc lengths, the actual size of the input body has no effect. After the mapping function has been determined, the scale factor is found by integrating  $\oint |dz/d\zeta| d\omega$  to determine the perimeter of the properly scaled body and comparing the result to the perimeter of the input body. It is possible to transform a body to a unit circle with the trailing edge of the body mapping to the point  $\zeta = 1$  on the circle and without affecting the angular orientation of distant portions of the field, only if the body is at a particular angle of attack. Since a change in angle of attack changes the values of all surface angles equally, and since only relative values of surface angle affect this method (because of the constraints imposed on the first coefficient in the series), the actual angular orientation of the input body has no effect. After the mapping function has been determined, the integral  $\oint \arg(dz/d\zeta) d\omega$  is evaluated. Since the result should be zero for the properly oriented body (as a consequence of the closure constraint), the value of the integral and Eq. (13) can be used together to determine the rotation angle.

#### Distortion of Other Bodies by the Single-Element Mapping

In addition to transforming one body to a unit circle, the single-element mapping also distorts the shapes of all nearby bodies. Equation (14) provides a means of calculating coordinates in the  $z$  plane, given coordinates in the  $\zeta$  plane. For present purposes, the reverse is required—a means of calculating coordinates in the  $\zeta$  plane, given coordinates in the  $z$  plane. Equation (14) can be reversed analytically to give a series for  $\zeta$  as a function of  $z$ , but the procedure for doing so is very costly, requiring a number of arithmetic operations proportional to the cube of the number of terms in the series. Furthermore, the series would be divergent over large regions near the body which was mapped to the unit circle ( $|z| < 1$ ).

A more efficient and reliable procedure is to treat Eq. (14) as a nonlinear equation with one unknown ( $\zeta$ ) and solve it by Newton-Raphson iteration. In most cases, the starting estimate for the calculations can be the converged solution for a neighboring point. For the first point on a body (or an isolated off-body point), however, such a solution is not available. In that case, an initial estimate is determined by solving the quadratic equation which results from neglecting all but the first three terms on the right-hand side of Eq. (14). Having determined the coordinates in the transformed plane, the mapping derivative is found directly from Eq. (9).

#### Convergence of the Multielement Mapping Procedure

The general procedure for transforming multiple airfoils to the same number of circles has been found to converge very rapidly. This is because the application of the corner-removing mappings makes the bodies nearly circular to begin with, and, once a body has been transformed to a circle, subsequent mappings of other bodies have only small effects. Figure 4 shows a typical example. The original geometry is a four-element, high-lift airfoil that was being considered for use on a future Douglas commercial aircraft. After the four corner-removing mappings, the bodies are irregular but roughly circular in shape. After only four single-element mappings (one per body), all bodies appear circular to the scale plotted. In this case, two additional mappings per body

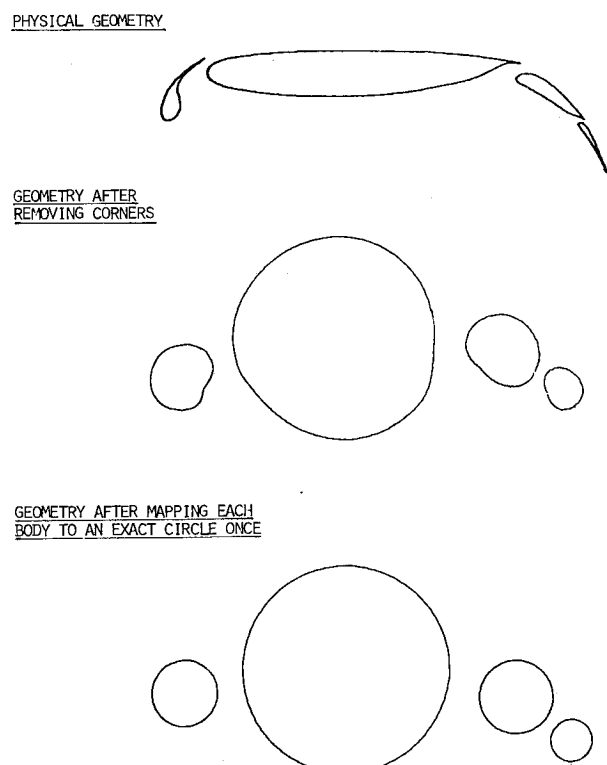


Fig. 4 Transformation of a four-element airfoil into four circles.

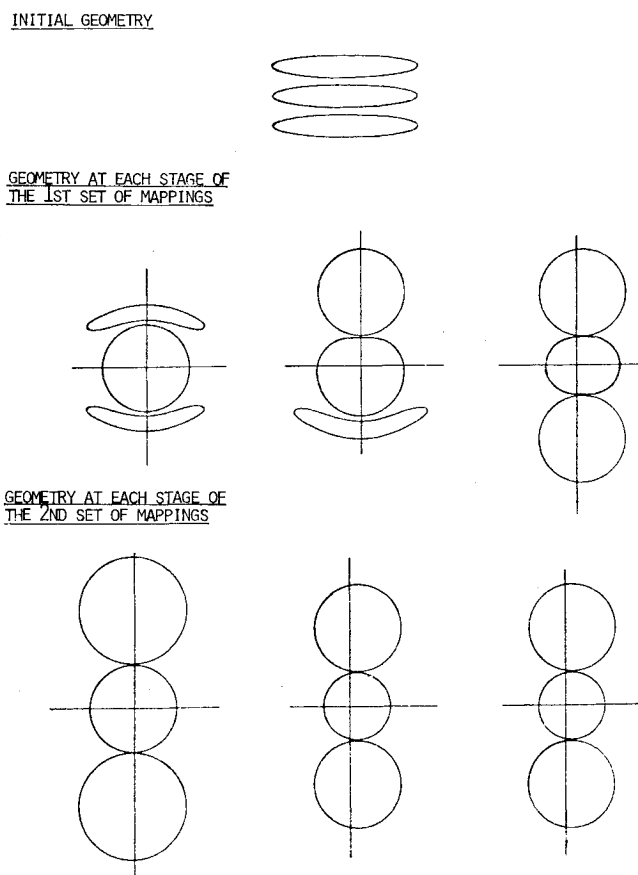


Fig. 5 Transformation of three ellipses to three circles.

were needed for the values of the mapping derivative at all points to converge to five significant figures.

Realistic multielement airfoils do not provide especially severe tests of the convergence of this multiple-body mapping technique, partly because the corner-removing mappings work so well, but mainly because the bodies are not close together over much of their length. A good measure of the severity of a test case is the distance between adjacent circles in the transformed plane. This distance is fairly large in the case of Fig. 4. More severe test cases were generated using closely-spaced ellipses with collinear minor axes. Figure 5 shows a three-element case, where mapping the first body to a circle causes the other bodies to partially wrap around the circle and mapping the second body to a circle significantly distorts the first circle. The resulting circles are very close together (not quite touching), but two sets of mappings (two mappings per body) produce bodies which appear perfectly circular to the scale shown. In this case, the fourth significant figure of the mapping derivative was not quite decided after five sets of mappings.

### Potential Flow Analysis of Multiple Circles

#### General Approach

The flow problem in the multiple-circle domain is more readily solved than the flow problem in the physical domain as a consequence of Milne-Thomson's<sup>12</sup> circle theorem which states, in essence, that a circle can be introduced into a flow having the complex potential  $\omega = f(\zeta)$  by altering the complex potential to

$$\omega = f(\zeta) + \bar{f}[r_0^2/(\zeta - \zeta_c)] \quad (15)$$

where  $\bar{f}$  represents the conjugate of the function  $f$ , and  $r_0$  and  $\zeta_c$  represent the radius and center, respectively, of the circle that is introduced into the flow. However, since the addition of a circle to the flow changes all the streamlines in the vicinity, an iterative approach is needed to introduce more than one circle into the flow. The procedure can be very similar in concept to the mapping procedure for multielement

airfoils. First, one circle is made a streamline of the flow, then another, and so on until each has been a streamline once. The process is then repeated as many times as needed until the streamlines follow the surfaces of the circles to within a sufficiently small tolerance.

Since the starting point in the preceding sequence of calculations is a uniform flow or the flow about a single circle, each application of the circle theorem can be regarded as the addition of discrete doublet and vortex image singularities. Using these basic ideas, Williams<sup>1</sup> developed a method for analyzing the flow about two circles. He applied this method in order to generate exact two-element airfoil test cases. More information on the flowfields produced by doublet and vortex singularities and formulas for the strengths and locations of their images can be found in Refs. 1 and 8. The present method does not reduce exactly to Williams' method for two-circle cases, although the results should be identical. To simplify the treatment of cases having more than two circles, the order of application of the singularities has been rearranged. To reduce the computational expense, intermediate steps of the procedure employ series expansions for the velocity field and do not calculate actual velocity values at any points on the circles. The present method is explained in more detail in the following sections.

#### Division of the Flow into Fundamental Solutions

The analysis of the flow about multiple circles is simplified and generalized by division of the flow into a number of fundamental solutions. This is a common technique in surface-singularity potential flow methods (see, for example, Ref. 13). The general flow is represented by a number of solutions equal to the number of circles plus two. The first two solutions have uniform flow at large distances from the circles, zero circulation at any point in the flow, and make use of doublet singularities in the numerical calculations. The first

solution has 0 deg angle of attack; the second has 90 deg angle of attack. These two solutions can be linearly superimposed to give the noncirculatory flow solution at any desired angle of attack. Each of the other fundamental flow solutions has stagnant flow at large distances from the circles, unit circulation about one circle (zero about the others), and makes use of vortex singularities in the numerical calculations. Application of the Kutta condition at the points corresponding to the trailing-edge points of the airfoils gives a set of linear algebraic equations (equal to the number of circles) to determine the proper multiple of each circulatory flow solutions in order to provide the final flow solution at a specified angle of attack.

#### Noncirculatory Flow Analysis Procedure

Each noncirculatory flow fundamental solution starts with a doublet at the center of each circle. The strength of each doublet is just sufficient to make its associated circle a streamline of the flow, in the absence of all other doublets. The next step is to place an image doublet within each circle for each doublet in each other circle. If  $NB$  is used to denote the total number of bodies, this step involves the addition of  $(NB-1)$  doublets in each circle. In the next step, an image doublet is placed within each circle for each doublet in each other circle that was added in the previous step. This step involves the addition of  $(NB-1)^2$  doublets in each circle. Additional steps are similar, except that each step involves the addition of a number of doublets equal to  $(NB-1)$ , raised to a power which is one higher than in the previous step.

In each step, the doublets get progressively weaker. After several steps, some of the doublets get so weak that their influence is negligible at all points on the circles. Further images descended from these doublets need not be computed. Therefore, in the last few steps of the process, the number of doublets decreases progressively until convergence is obtained.

Even though the process converges rapidly, the total number of doublets can become very large (sometimes several hundred), making it unfeasible (or at least uneconomical) to calculate the velocity field induced by the set of doublets, especially if this must be done at each step in order to evaluate the extent of convergence of the process. To avoid this, the complex velocity due to all the doublets within a given circle is expanded in a Laurent series about the center of the circle. It has been found that an essentially exact representation of the influence of several hundred singularities can be obtained using about twenty terms in the series. Addition of doublets at each step thus involves only modification of the coefficients of the series expansions. Convergence is indicated when the coefficients stop changing from step to step.

#### Circulatory Flow Analysis Procedure

Each circulatory flow fundamental solution starts with a single point vortex of unit strength at the center of one circle and no other singularities in any of the bodies. The next step is to place a pair of counterrotating vortices in each circle, other than the circle with the single point vortex. One member of each pair cancels out the induced normal flow due to the point vortex; the other cancels out the change in circulation due to the first. The next step involves the addition of a pair of counterrotating vortices in each circle for each of the vortex pairs added in each other circle in the previous step. The calculations proceed in a manner very similar to those in the noncirculatory flow analysis method. Because of the asymmetry of the starting condition, the rate of growth of the number of singularities is not identical to the noncirculatory case, but is roughly similar. Vortex images do not decrease in strength like doublets do, but the images of vortex pairs get closer together at a rate approaching the rate of decrease of the strength of doublet images for closely spaced pairs. Convergence characteristics of the circulatory and non-circulatory fundamental solutions are, therefore, very similar.

As in the noncirculatory cases, series expansions for the complex velocity are employed in order to avoid having to calculate the velocity fields of a large number of individual singularities or singularity pairs.

#### Convergence of the Flow Analysis Procedure

The multiple-circle flow analysis procedure is rapidly convergent—generally requiring the application of between six and twenty sets of singularities for each fundamental flow to be calculated to five-digit accuracy. The number of arithmetic operations required in each step is generally very small compared to the number needed to transform the airfoils to the circles (even if several hundred singularities are needed). The flow analysis calculations, therefore, usually account for less than about 30% of the total computational expense of a complete potential flow calculation.

#### Calculated Results

In order to assess the accuracy of the calculated results, comparisons were made with some exact two-element airfoil solutions generated by James<sup>2</sup> by distributing poles in the interior of two circles. A case resembling a realistic airfoil-slat combination is shown in Fig. 6. Using the coordinates provided by James' method (145 points per airfoil element), no deviations between the the exact and calculated results are detectable at the scale shown. A more severe test case, also generated by James, is shown in Fig. 7. In this case, a bump has been deliberately introduced into the region of the main airfoil element immediately adjacent to the slat. Using the coordinates provided by James' method, only small inaccuracies can be detected in the regions very close to the bump. In both these cases, 129 points have been used to represent each circle.

A more realistic example is provided by the four-element airfoil shown earlier (Fig. 4). In this case, the geometry of the main airfoil element is specified by 101 defining points; each other element has 81 points. In the mapping calculations, each

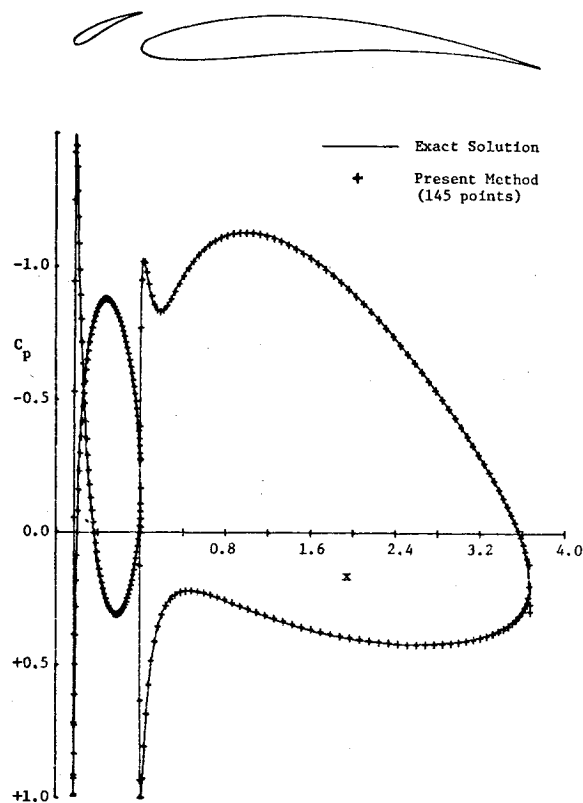


Fig. 6 Accuracy of the calculated pressure distributions (James' airfoil-slat case).

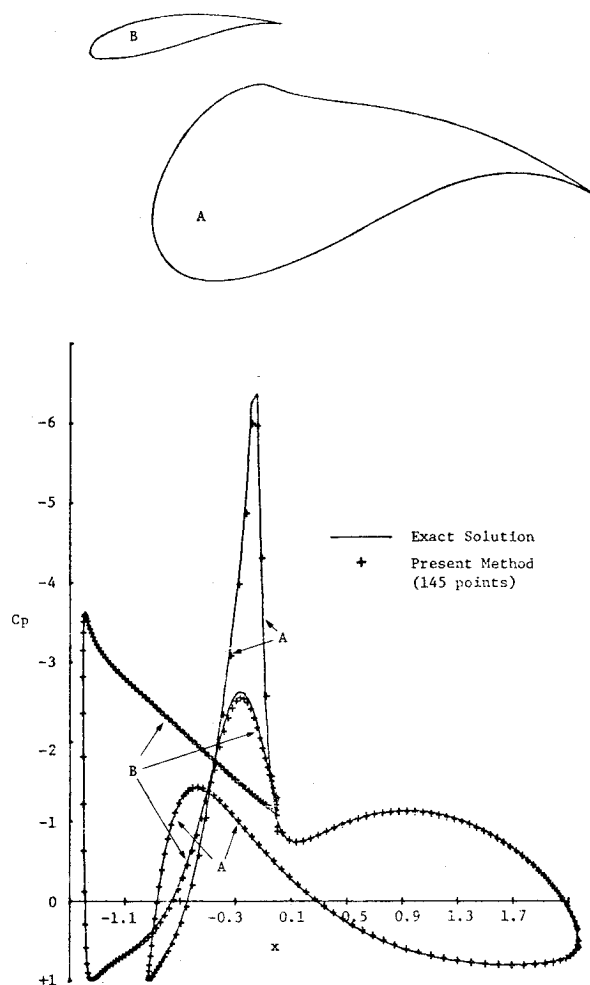


Fig. 7 Accuracy of the calculated pressure distributions for a more extreme case (James' two-element body with bump).

circle is represented by 65 points. Since no exact solution exists for this case, comparison is made with the results of the higher-order surface-singularity method of Hess.<sup>13</sup> Figure 8 shows that the mapping method and the surface-singularity method give essentially identical results.

Since the initial motivation for this work was to bring about a substantial reduction in the computational expense of potential flow calculations for multielement airfoils, it is interesting to compare the costs of the calculations using the present method and Hess' method. However, such comparisons are very difficult to interpret. The most common standard of computational effort is the computer CPU time. This quantity depends strongly on the particular machine, time of day, input/output considerations, and programming style, as well as number of arithmetical and logical operations to be performed. Thus, precise comparisons are not possible. Better comparisons can be made if both methods are computed on the same machine at about the same time. For the four-element case, the mapping method was faster than the surface-singularity method by a factor of 8.4. This should be considered as a very preliminary (but encouraging) result. It is possible that adequate accuracy could have been obtained in the surface-singularity case using fewer elements in the geometry and singularity discretizations—thus significantly reducing the cost factor. An undesirable result of this, however, would be the reduced resolution in regions where the solution varies rapidly. It is also possible that future refinements in the mapping procedure could reduce the expense of the mapping calculations—thus significantly increasing the cost factor.

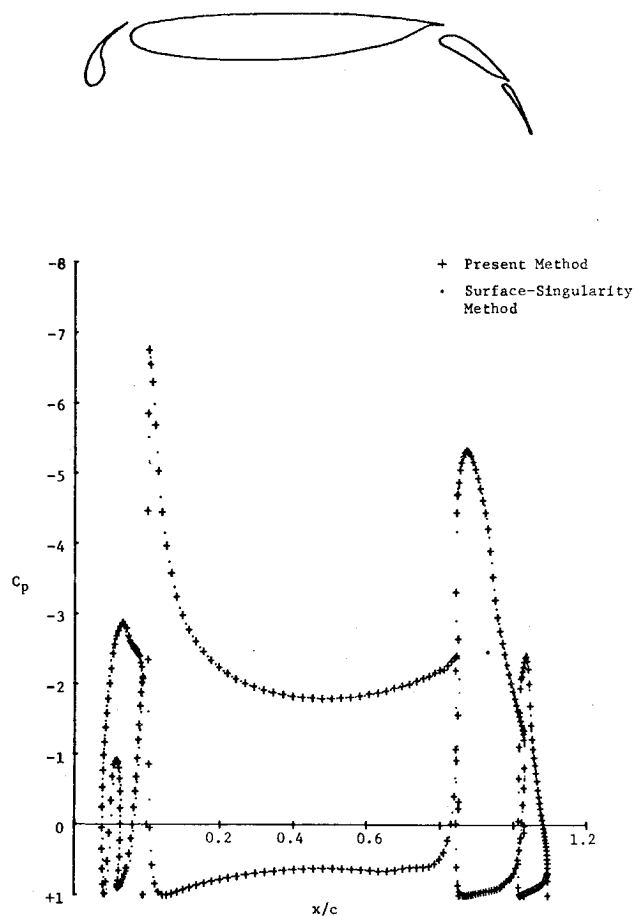


Fig. 8 Comparison of the results of the mapping method and a distributed-singularity method for a four-element airfoil.

## Conclusions

The goal of the research described in this article has been to develop a potential flow method for general multielement airfoils using conformal mapping and to demonstrate its accuracy and efficiency. That goal has been substantially achieved. Specific conclusions resulting from this effort include:

- 1) The mapping of multiple bodies to the same number of circles by the successive application of a single-body mapping is a rapidly convergent procedure.
- 2) High accuracy can be maintained throughout the mapping process provided enough terms are retained in the truncated series for the mapping functions and provided certain precautions are taken in the numerical procedures.
- 3) The mapping process is very efficient to compute, provided a single-body mapping which makes use of Fast Fourier Transforms is employed.
- 4) The analysis of multiple circles using multiply-reflected image singularities is also a rapidly convergent process.
- 5) The multiple-circle analysis method is also very efficient to compute, provided the velocity at each point is not calculated at intermediate steps of the procedure.
- 6) The overall potential flow method gives results of very high accuracy.
- 7) The overall potential flow method may be substantially more efficient to compute than a surface-singularity method.

## Acknowledgment

This research was conducted under the Independent Research and Development Program of the McDonnell Douglas Corporation.

### References

- <sup>1</sup>Williams, B. R., "An Exact Test Case for the Plane Potential Flow About Two Adjacent Lifting Airfoils," RAE Tech. Rept. 71197, 1971.
- <sup>2</sup>James, R. M., "Analytical Studies of Two-Element Airfoil Systems," Douglas Aircraft Company Rept. MDC J5831, 1974.
- <sup>3</sup>Theodorsen, T., "Theory of Wing Sections of Arbitrary Shape," NACA Rept. 411, 1932.
- <sup>4</sup>James, R. M., "A New Look at Two-Dimensional Incompressible Airfoil Theory," Douglas Aircraft Company Rept. MDC J0918/01, 1971.
- <sup>5</sup>Garrick, T. E., "Potential Flow About Arbitrary Biplane Wing Section," NACA Rept. 542, 1936.
- <sup>6</sup>Ives, D. C., "A Modern Look at Conformal Mapping Including Multiply Connected Regions," *AIAA Journal*, Vol. 14, Aug. 1976, pp. 1006-1011.
- <sup>7</sup>Cooley, J. W. and Tukey, J. W., "An Algorithm for the Machine Calculation of Complex Fourier Series," *Math. of Comp.*, Vol. 19, No. 90, 1965.
- <sup>8</sup>Halsey, N. D., "Potential Flow Analysis of Multiple Bodies Using Conformal Mapping," Long Beach Masters' Thesis, California State University, 1977.
- <sup>9</sup>Nehari, Z., *Conformal Mapping*, McGraw-Hill Book Co., Inc., New York, 1952.
- <sup>10</sup>Bauer, F., Garabedian, P., Korn, D., and Jameson, A., *Supercritical Wing Sections, II. Lecture Notes in Economics and Mathematical Systems*, Vol. 108, Springer-Verlag, New York, 1975.
- <sup>11</sup>Sells, C. C. L., "Plane Subcritical Flow Past a Lifting Airfoil," RAE Tech. Rept. 67146, 1967.
- <sup>12</sup>Milne-Thomson, L. M., *Theoretical Hydrodynamics*, Macmillan Co., New York, 1967.
- <sup>13</sup>Hess, J. L., "Higher Order Numerical Solution of the Integral Equation for the Two-Dimensional Neumann Problem," Douglas Engineering Paper 6060, 1972.

*From the AIAA Progress in Astronautics and Aeronautics Series . . .*

## REMOTE SENSING OF EARTH FROM SPACE: ROLE OF "SMART SENSORS"—v. 67

*Edited by Roger A. Breckenridge, NASA Langley Research Center*

The technology of remote sensing of Earth from orbiting spacecraft has advanced rapidly from the time two decades ago when the first Earth satellites returned simple radio transmissions and simple photographic information to Earth receivers. The advance has been largely the result of greatly improved detection sensitivity, signal discrimination, and response time of the sensors, as well as the introduction of new and diverse sensors for different physical and chemical functions. But the systems for such remote sensing have until now remained essentially unaltered: raw signals are radioed to ground receivers where the electrical quantities are recorded, converted, zero-adjusted, computed, and tabulated by specially designed electronic apparatus and large main-frame computers. The recent emergence of efficient detector arrays, microprocessors, integrated electronics, and specialized computer circuitry has sparked a revolution in sensor system technology, the so-called smart sensor. By incorporating many or all of the processing functions within the sensor device itself, a smart sensor can, with greater versatility, extract much more useful information from the received physical signals than a simple sensor, and it can handle a much larger volume of data. Smart sensor systems are expected to find application for remote data collection not only in spacecraft but in terrestrial systems as well, in order to circumvent the cumbersome methods associated with limited on-site sensing.

505 pp., 6 × 9, illus., \$22.00 Mem., \$42.50 List

TO ORDER WRITE: Publications Dept., AIAA, 1290 Avenue of the Americas, New York, N. Y. 10019